Kingdom of Saudi Arabia
Imam Mohammad Ibn Saud Islamic University (IMSIU)
Faculty of Sciences – Department of Physics

Low temperature photoluminescence (PL) study of heterostructure nanocolumns

A graduation project submitted to the Department of Physics in partial fulfillment of the requirements for the degree of Bachelor of Science in Applied Physics

by

Lubna Alhaidari

Norah Alhanaki

Supervisor/s

Dr. Naglaa Abdel All

IMSIU-Riyadh-KSA

May, 2025

TABLE OF CONTENTS

ACKNOWLEDGMENT

الحمد لله حمداً كثيراً طيباً مباركاً فيه، كما ينبغي لجلال وجهه وعظيم سلطانه. والصلاة والسلام على أشرف الأنبياء والمرسلين نبينا محمد وعلى آله وصحبه آجمعين.

بكل شرف وامتنان نهدي هذا المشروع إلى من تفيئنا نعيم ظلهما.. واستهدينا بنور بصيرتهما والدينا الكريمين، وأسرتنا العزيزة.

نتقدم بخالص الشكر وجزيل الامتنان لكل من ساندنا وقومنا في مراحل هذا المشروع، وعلى رأسهم سعادة الدكتورة نجلاء عبدالعال التي تفضلت علينا بالإشراف على المشروع، ثم ما فتئت تقومنا وترشدنا وتصوبنا، فلها منا كل الدعوات وأطيبها.

ونزجي الشكر لكلية العلوم، ولقسم الفيزياء، ولأستاذتنا الكريمات، ولكل من تفضل بالتوجيه والإرشاد.

والشكر موصول لزميلاتنا العزيزات، ولكل من شجعنا، وساندنا.

والحمد لله الذي بنعمته تتم الصالحات.

Abbreviation & Acronym

Zero-Dimension (0D)

One-Dimension (1D)

Two-Dimension (2D)

Gallium Nitrite (GaN)

Wide band gap (WBG)

Photoluminescence (PL)

Cathodoluminescence (CL)

High electron mobility spectroscopy (HEMTs)

Two-dimensional electron gas (2DEG)

Plasma-assisted molecular beam epitaxy (PA-MBE)

Radio frequency (RF)

High-resolution scanning electron microscope (HR-SEM)

High-resolution transmission electron microscope (HR-TEM)

Reflection high-energy electron diffraction (RHEED)

X-ray diffraction (XRD)

Nanorods (NRs)

Continues-wave (CW)

Single Quantum (SQ)

LIST OF TABLES

LIST OF FIGURES

ABSTRACT

Gallium nitride (GaN) is a semiconductor material and one of the most important materials in the semiconductor applications. $Al_{0.12}Ga_{0.88}N/GaN/Al_{0.12}Ga_{0.88}N/Si$ heterostructure nanocolumns were grown under plasma assisted molecular beam epitaxy (PA-MBE). This study investigates its optical properties by studying the photoluminescence (PL) spectra at low temperature according to the growth of single quantum disk (SQ) inserted between AlGaN layers. The morphological and structural examination was obtained using scanning electron microscopy (SEM), transmission electron microscopy (TEM), reflection high-energy electron diffraction (RHEED), and X-ray diffraction (XRD). The photoluminescence spectra were measured using a continuous wave He–Cd laser with a wavelength of 325 nm, and a closed-cycle helium cryostat was used to cool the sample down to 10 K. The results were compared with GaN and AlN/GaN nanorod samples where it measured at the same temperature. The strain effect is reduced in the growth of its layers due to the small mismatch in the unit cell between GaN and AlGaN. Also, GaN single quantum disk shows new emission which is very useful for many optoelectronic applications.

الملخص العربي

نيتريد الجاليوم (GaN) مادة شبه موصلة ويعد من أكثر المواد أهمية في العديد من تطبيقات أشباه الموصلات. تم بناء أعمدة نانوية متغايرة البنية من $Al_{0.12}Ga_{0.88}N/GaN/Al_{0.12}Ga_{0.88}N/Si$ باستخدام تقنية التراكب الجزيئي بمساعدة البلازما (PA-MBE). تتناول هذه الدراسة خصائص الأعمدة البصرية من خلال دراسة أطياف التلألؤ الضوئي (PL) عند درجات حرارة منخفضة، وفقًا لنمو القرص الكمي المُدرج بين طبقات AlGaN. تم إجراء الفحص البنيوي والمورفولوجي باستخدام المجهر الإلكتروني الماسح (SEM)، والمجهر الإلكتروني النافذ (TEM)، وانعكاس الإلكترونات عالية الطاقة (RHEED)، وحيود الأشعة السينية (XRD). تم قياس أطياف التلألؤ الضوئي باستخدام ليزر He–Cd ذو موجة مستمرة بطول موجي 325 نانومتر، واستُخدم جهاز تبريد هيليوم مغلق الدورة لتبريد العينة إلى 10 كلفن. لتفسير النتائج ومناقشتها تم مقارنة النتائج بعينات من GaN وAlN/GaN النانوية والتي تم قياسها عند نفس درجة الحرارة. تم ملاحظة انخفاض تأثير الانفعال في نمو طبقات الاعمدة النانوية بسبب التوافق في خلية الوحدة بين GaN وAlGaN. حيث أُظهر قرص GaN الكمي المفرد انبعاثًا جديدًا، وهو مفيد جدًا للعديد من التطبيقات البصرية الإلكترونية.

Chapter 1

Theoretical background and Literature review

1.1 Introduction

The field of study known as nanoscience is concerned with the characteristics of matter at the nanoscale, with a focus on the special, size-dependent characteristics of solid-state materials. Nanomaterials are now becoming important for the overall development of mankind. Nanomaterials are substances that are between 1 and 100 nm in size, at least in one of the three dimensions in nanoscales [1]. Due to the increase of surface to volume ratio, nanomaterials have special optical, magnetic, electrical, and physical, reactivity, strength, surface area, sensitivity, and stability features. For a material to be classified as nanomaterial, at least one dimension must be 100 nm or less. Therefore, nanomaterials are classified into three types based on their size dimensions: Zero-Dimension (0D), One-dimension (1D) and Two-dimension (2D) as shown in Figure (1.1) [1].

- **Zero-dimensional nanomaterials:**

  These nanomaterials have all three dimensions (x, y, and z) within the nanoscale range or are not dimensional outside the Nano metric range (>10 nm). They can be amorphous or crystalline, single crystalline or polycrystalline, exhibiting various shapes and forms. e.g., gold nanoparticles.

- **One-dimensional (1-D):**

  ID nanomaterials: Nanomaterials in this class have two of their three dimensions (x, y) in the nanoscale range, but one dimension of the nanostructure is outside the non-metric range (>10 nm). They can be amorphous or crystalline, single crystalline. e.g., GaN nanowires.

- **Two-dimensional (2-D):**

  2D nanomaterials have plate-like shapes with two dimensions outside the nanometer range, but 1D (x) is at the nanoscale (between 1 and 100 nm). 2D nanomaterials can be amorphous or crystalline, metallic. e.g., TiO_2 nanosheets.

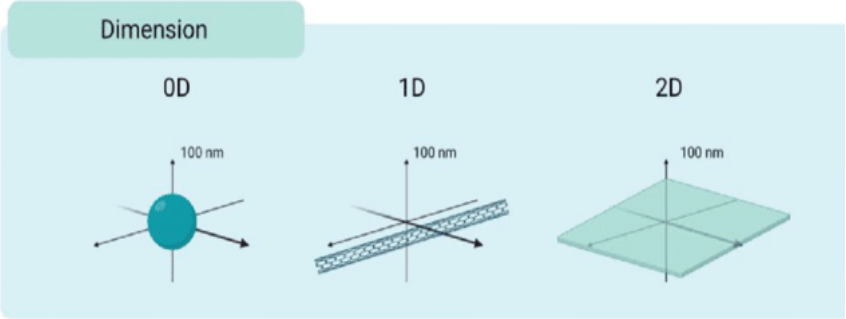

Fig. (1.1): nanomaterials based on their dimension.

The study and application of nanomaterials have been useful in many various fields, in science, medicine, and technology.

1.2 Crystals and Crystallography

Crystals are solids that possess long-range order. The arrangement of the atoms at one point in a crystal is identical, (excepting localized mistakes or defects that can arise during crystal growth), to that in any other remote part of the crystal. Crystallography describes the ways in which the component atoms are arranged in crystals and how the long-range order is achieved. A central concept in crystallography is that the whole crystal can be built up by stacking identical copies of the unit cell in the same orientation. That is to say, crystal is characterized by both translational and orientational long-range order. The unit cells are displaced repeatedly in three dimensions, (translational long-range order), without any rotation or reflection, (orientational long-range order). The edges of the unit cell are generally considered part of the crystal lattice, which is an infinite pattern of points. However, for crystallographic purposes, it is most convenient to choose the smallest possible unit cell that reveals the symmetry of the lattice [2].

There are only 14 possible three-dimensional lattices, called Bravais lattices (Fig. 1.2). Bravais lattices are sometimes called direct lattices. Bravais lattices are defined in terms of conventional crystallographic bases and cells. The rules for selecting the preferred lattice are determined by the symmetry of the lattice. Based on these orderly arrangements, crystals are classified into seven crystal

systems that. The crystal systems are sets of reference axes, which have direction as well as a magnitude, and hence are vectors. The crystal families and classes are given in Table (1.1).

Crystal family	Crystal system	Axial relationships
Isometric	Cubic	$a = b = c, \quad \alpha = \beta = \gamma = 90^\circ;$
Tetragonal	Tetragonal	$a = b \neq c, \quad \alpha = \beta = \gamma = 90^\circ;$
Orthorhombic	Orthorhombic	$a \neq b \neq c, \quad \alpha = \beta = \gamma = 90^\circ;$
Monoclinic	Monoclinic	$a \neq b \neq c, \quad \alpha = 90^\circ, \beta \neq 90^\circ, \gamma = 90^\circ;$
Anorthic	Triclinic	$a \neq b \neq c, \quad \alpha \neq 90^\circ, \beta \neq 90^\circ, \gamma \neq 90^\circ;$
Hexagonal	Hexagonal	$a = b \neq c, \quad \alpha = \beta = 90^\circ, \ \gamma = 120^\circ;$
	Trigonal or Rhombohedral	$a = b = c, \quad \alpha = \beta = \gamma;$ or $a' = b' \neq c', \alpha' = \beta' = 90^\circ, \gamma' = 120^\circ;$ (hexagonal axes)

Table (1.1): The seven-crystal system.

The three reference axes are labelled a, b and c, and the angles between the positive direction of the axes are α, β and γ as shown in Fig. (1.3). In figures, the a-axis is represented as projecting out of the plane of the page, towards the reader, the b-axis points to the right and the c-axis points towards the top of the page. be parallel to the axial vectors a, b and c, of the seven crystal systems. The lengths of the unit cell sides are written a, b and c, and the angles between the unit cell edges are written, α, β and γ. The collected values a, b, c, α, β and γ for a crystal structure are termed the unit cell or lattice parameters.

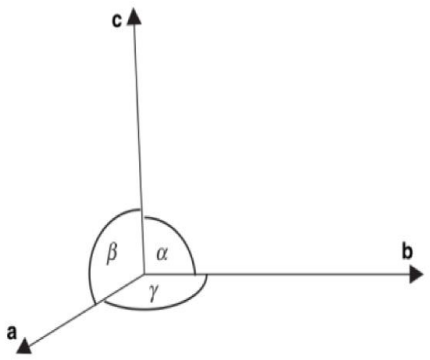

Fig. (1.2): unit cell sides are written a, b and c, and the angles between the unit cell edges are written, α, β and γ.

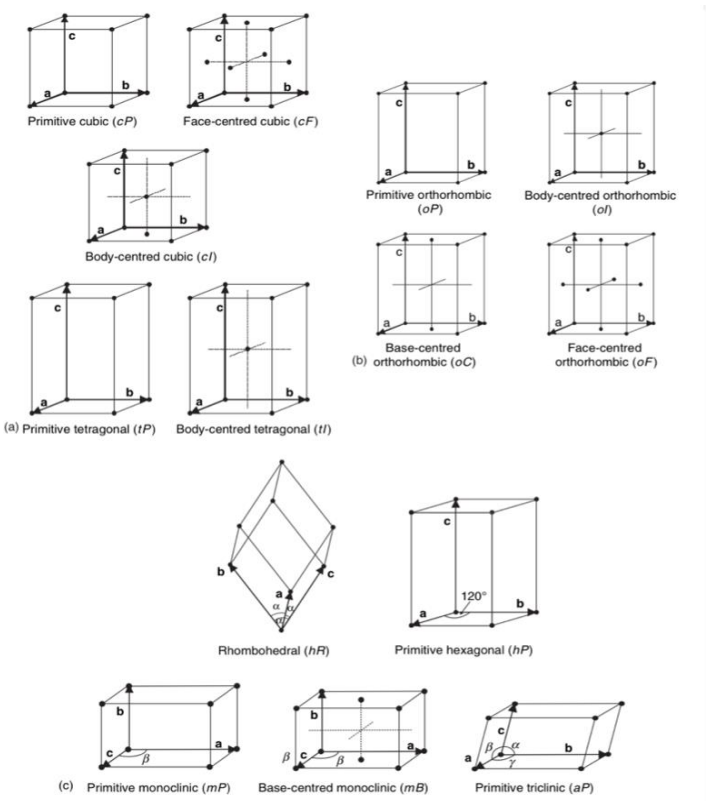

Fig. (1.3): The 14 Bravais lattices.

The minimum amount of information needed to specify a crystal structure is the unit cell type, i.e., cubic, tetragonal, etc, the unit cell parameters and the positions of all of the atoms in the unit cell. The atomic contents of the unit cell are a simple multiple, Z, of the composition of the material. The value of Z is equal to the number of formula units of the solid in the unit cell. Atom positions are expressed in terms of three coordinates, x, y and z [2].

1.3 Gallium nitrate

Gallium nitride (GaN) is a compound with a direct bandgap semiconductor and made of Gallium and Nitrogen elements that forms a crystalline structure. Belongs to Nitride semiconductors (GaN, AlGaN, InAlN, InGaN, InAlGaN, AlN, etc.) possess several properties, which make them very useful for many opto- electronic and microelectronic applications.[3]

Table (1.2) reports the main physical properties of GaN and other nitrides in comparison with other semiconductors, highlighting some implications in material growth, optoelectronics, and power- and high-frequency electronics. As can be seen, these materials exhibit several advantages for

optoelectronic and power electronics, mainly related to their direct band gap, or the wide band gap (WBG) and high critical field. However, there are also several features which make material growth and the technology of devices very difficult.

	Property	Value/range	Comparison with other semiconductors
	Build-in internal electric field	Up to 2 MV/cm (InGaN/GaN)	The strong build-in internal electric field increases the spatial separation of electrons and holes, thus reducing the efficiency of radiative recombination in optoelectronic devices
Power/high-frequency (HF) electronics	Wide band gap, E_g	From 3.4 eV (GaN) to 6.1 eV (AlN)	Possible applications of GaN-based materials in high-voltage, high-power, and high-temperature electronics, in competition with SiC (and possibly in future, with Ga_2O_3 and diamond). The high defects density still hinders the full exploitation of the electric field strength
	Critical electric field, E_{CR}	3–3.75 MV/cm (GaN)	
	Electron affinity, χ	3.1–4.1 eV (GaN)	
	Dielectric constant, ε_r	9.5 (GaN)	
	Intrinsic carrier concentration, n_i	$\approx 10^{-10}$ cm^{-3} (GaN) at room temperature	Low leakage currents and high operation temperatures are possible, if the GaN material quality is improved
	Electron saturation velocity, v	3×10^7 cm/s (GaN)	Enable the fabrication of devices operating at high frequencies, in competition with the traditional GaAs technology
	Electron mobility, μ_n	1100–2000 cm^2/V s (GaN, AlGaN/GaN)	
	Thermal conductivity, κ	1.3–2.1 W/cm K (GaN)	Comparable to Si but significantly lower than SiC and diamond, making the heat dissipation a concern for GaN-based power devices

Table (1.2): Physical properties of GaN and other nitrides in comparison with other semiconductors.

For GaN, the wurtzite crystal structure is schematically depicted in Fig. (1.4), where the unit cell, highlighted with bold lines, is characterized by the lattice parameters a (3.19Å) and c (5.19Å) [3]. The Ga and N atoms are arranged in two interpenetrating hexagonal closely packed lattices, with a shift of 3/8 c. In the hexagonal wurtzite structure, GaN has no inversion symmetry in the [001] direction (the so-called c-axis). For that reason, it is possible to distinguish two different orientations of GaN crystals, i.e. the Ga-face (Figure 1.4a) and the N-face (Figure1.4b), depending on whether the material is grown with Ga or N on top. These two faces have different chemical properties: Ga-face is more chemically inert and may behave differently during growth (e.g. the Ga-face incorporates easier acceptors, whereas the N-face incorporates easier donors). The covalent bonds allow each atom to be tetahedrally bonded to four atoms of the other type.

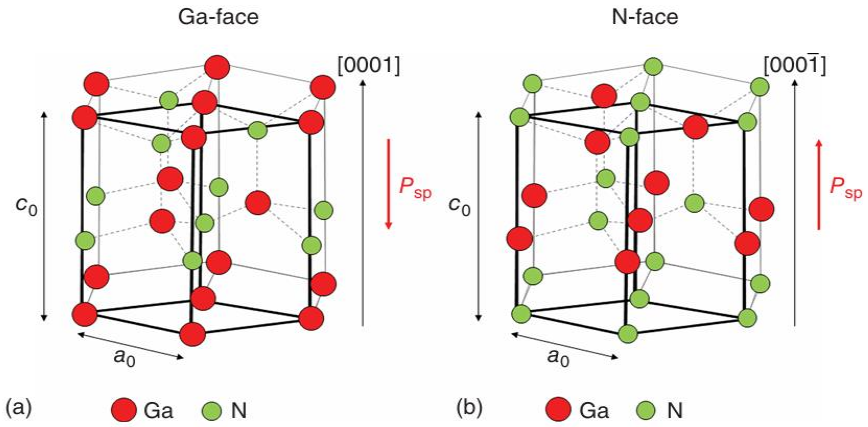

Fig. (1.4): Hexagonal crystal structure of GaN. (a) Ga-face (b) N-face.

The scientific and technological achievements were made in nitride-based optoelectronic devices since the 1980s had leading to the creation of new multibillion markets. Fig. (1.5) illustrates the examples of consumer applications of nitride-based optoelectronic devices, i.e. LEDs and LDs, in several fields (general lighting, cars, video projections, etc.). Although GaN-based devices have already entered our daily life, there are still many problems related to material growth and device processing that deserve further intensive research.

Fig. (1.5): Examples of applications of nitrides devices (LEDs and LDs) in optoelectronics.

1.4 Literature review

Akar et al. (2024) studied the Fabrication of Tapered and Cylindrical GaN Nanowires Using Nanosphere Lithography. This paper presents a comprehensive study on the fabrication of GaN

nanowires using a top-down approach facilitated by nanosphere lithography. We focus on optimizing both dry and wet etching processes to achieve high-aspect-ratio nanowires with controlled shapes. The final wet etching step, critical for shaping the nanowires, was performed with a crystallography-selective method, resulting in nanowires with vertical m-plane facets or tapered structures, depending on the initial diameter of the spheres. This demonstrates the process's adaptability to control nanowire geometry [4] .

Akar et al. (2023) studied the Ultraviolet Photodetectors based on GaN and AlGaN/AlN Nanowire Ensembles: Effects of Planarization with Hydrogen Silsesquioxane and Nanowire Architecture. Here, we report a comprehensive study on UV photodetectors based on GaN or AlGaN/AIN nanowire ensembles encapsulated in HSQ. We show that this material is efficient for passivating the nanowire surface, it introduces a compressive strain in the nanowires and preserves their radiative efficiency. We discuss the final performance of planarized UV photodetectors based on three kinds of nanowire ensembles: (i) non-intentionally doped (nid) GaN nanowires, (ii) Ge-doped GaN nanowires, and (iii) nid GaN nanowires terminated with an AlGaN/AIN superlattice [5].

Michael A. Reshchikov (2022) studied the Photoluminescence (PL) bands in GaN associated with point defects involving nitrogen or gallium vacancy (VN or VGa). The VN-containing defects, including the isolated VN and its complexes with acceptors, are often observed in PL from semi-insulating GaN and are responsible for the green (GL2) and red (the RL2 family) bands. The complexes of the VGa with hydrogen and oxygen are abundantly formed in n-type GaN grown by the Ammon thermal method. Some of these complexes are responsible for PL bands in the red-yellow region of the PL spectrum. [6]

Lawrence et al. (2007) studied GaN nanowires with diameters of 50–250 nm, grown by catalyst-free molecular beam epitaxy, were characterized by photoluminescence PL and cathodoluminescence CL spectroscopy at temperatures from 3 to 297 K, and high-resolution x-ray diffraction HRXRD at 297 K. The lattice parameters of the nanowires, determined by HRXRD, are in good agreement with recent measurements of freestanding quasisubstrates; the relative variation of the lattice parameters between the nanowires and quasisubstrates is $\leq 2 \times 10^{-4}$. Both as-grown samples, which contained nanowires oriented normal to the substrate as well as a rough, faceted matrix layer, and dispersions

of the nanowires onto other substrates, were examined by PL and CL. The D0XA line at 3.472 eV, ascribed to excitons bound to shallow donors, was observed in low-temperature PL and CL; free-exciton lines (XA at ≈3.479 eV, XB at ≈3.484 eV) were observed in PL at temperatures between 20 and 80 K. The linewidth of the D0XA peak was larger in PL spectra of the nanowires than in quasisubstrates. The broadening of the D0XA peak in PL of the nanowires is tentatively ascribed to inhomogeneous stress/strain. In addition, the D0XA peak was significantly broader in CL than in PL spectra of the same nanowire samples. The further large broadening of the CL peak (as compared to PL) is tentatively ascribed to Stark effect broadening, induced by the electric fields of trapped charges that are created in the CL excitation process [7].

A. Wojcik et al. (2002) studied the results of photoreflectance spectroscopy (PR) of undoped GaN/AlGaN heterostructures used for fabrication of high electron mobility transistors (HEMTs). For proper operation of such devices a triangular quantum well created at the interface between GaN and AlGaN is required. Due to spontaneous and piezoelectric polarisation-induced electric fields in GaN/AlGaN heterostructures, free electrons are accumulated close to the interface forming a two-dimensional electron gas (2DEG). Aluminium composition in AlGaN can be determined from PR and thus the obtained data allow for estimation of the shape of 2DEG confinement potential which is necessary for verification of design assumptions and control of growth process [8].

Chapter 2

Experimental techniques in the heterostructure nanocolumn

2.1 Sample growth

AlxGa1-xN (10 nm)/GaN (3 nm)/AlxGa1-xN (10 nm)/GaN (30 nm) nanocolumns with x = 0.12 were grown on Si substrates that had a thin native SiO_2 layer (about 2 nm thick), as shown in Figure (2.1) using plasma-assisted molecular-beam epitaxy (PA-MBE) shown in Figure (2.2). The nanocolumns were grown in nitrogen-rich conditions using radio frequency (RF) plasma-enhanced N_2. The Ga flux (1.0×10^{-8} Torr), N_2 flow rate (1.0 sccm), and RF plasma power (300 W) were fixed. The process started by thermally cleaning the Si substrates at 800 °C for 15 min. Then, a low-temperature GaN buffer layer grew at 450 °C for 40 s, followed by annealing at 800 °C for 10 min in the plasma-activated nitrogen atmosphere. [9]

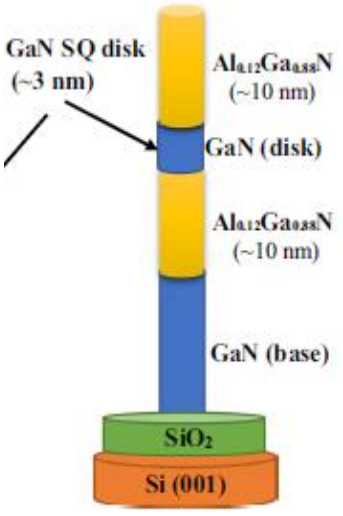

Fig. (2.1): Schematic diagram of AlxGa1-xN (10 nm)/GaN (3 nm)/AlxGa1-xN (10 nm)/GaN (30 nm) nanocolumns.

After that, GaN nanorods were grown at 800 °C followed by the growth of $Al_{0.12}Ga_{0.88}N$, GaN, and $Al_{0.12}Ga_{0.88}N$ alloys to make the designed single quantum disk nanocolumns. The Al concentration (x) was kept around 12% during the growth of $Al_{0.12}Ga_{0.88}N$, which was done by adjusting the ratio between Al and Ga vapor pressures [9]. The growth rate was controlled by changing the III/V ratio to achieve a rate of about 1.5 μm/h.[9]

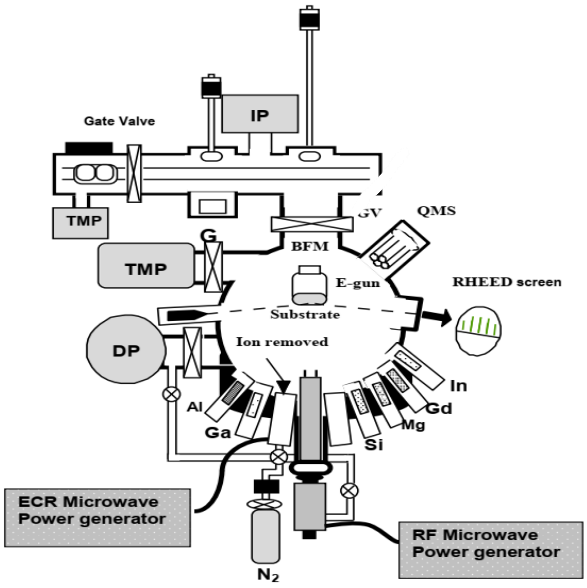

Fig. (2.2): Plasma-assisted molecular-beam epitaxy (PA-MBE) for sample growth.

2.2 Morphological and structural investigations

Morphological and structural investigations of the grown $Al_{0.12}Ga_{0.88}N/GaN/Al_{0.12}Ga_{0.88}N$ nanocolumns were examined using high-resolution scanning electron microscope (HR-FE-SEM), high-resolution transmission electron microscopy (HR-TEM), Reflection High-Energy Electron Diffraction (RHEED), and X-ray diffraction (XRD).

2.2.1 High-Resolution Field Emission Scanning Electron Microscope (HR-FE-SEM)

Scanning Electron Microscopy (SEM) is a type of electron microscope that produces images of a sample by scanning its surface with a focused beam of electrons as shown in Figure (2.3).

An electron source emits electrons that are accelerated by an applied voltage. These electrons pass through magnetic lenses, which converge the stream into a focused beam that strikes the sample surface in a precise spot. The electron detector collects the emitted electrons from the sample then can be converted into electrical signals.

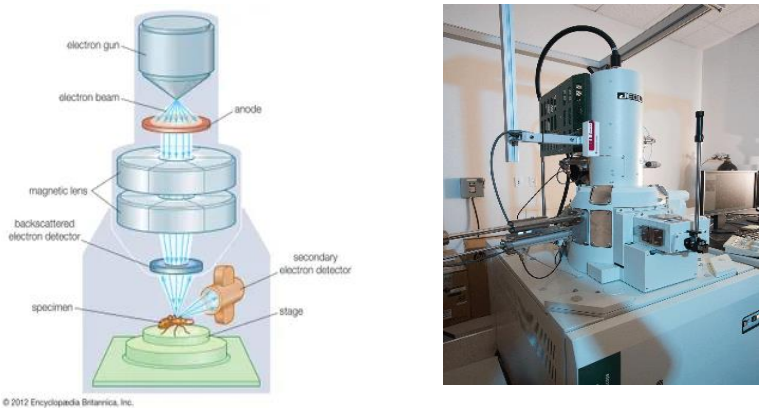

Fig. (2.3): Schematic diagram of scanning electron microscope (left) and SEM device (right).

2.2.2 High-Resolution Transmission Electron Microscopy (HR-TEM)

It is a microscopy technique in which a beam of electrons is transmitted through a specimen to form an image to check the single nanocolumnar structure as shown in Figure (2.4). An electron source emits electrons that are accelerated by an applied voltage. These electrons pass through magnetic lenses, which converge the stream into a focused beam that beam passes through the sample, where the electrons are either scatter or hit a fluorescent screen at the bottom of the microscope to produce the image.

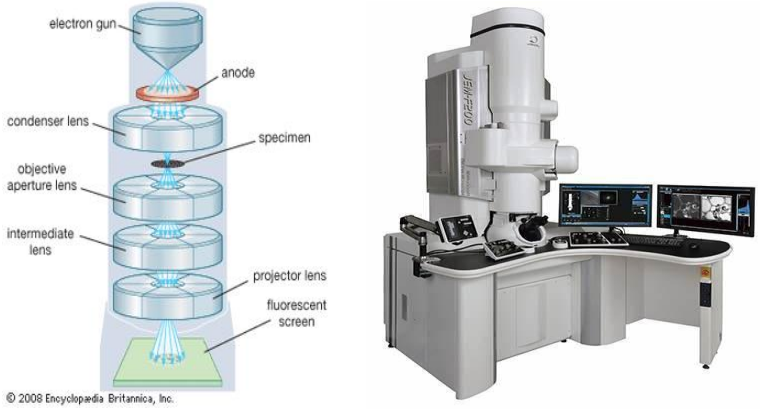

Fig. (2.4): Schematic diagram of transmission electron microscope (left) and TEM device (right).

2.2.3 Reflection high-energy electron diffraction (RHEED)

It is a surface-sensitive characterization technique that operates by directing high-energy electrons at a shallow angle toward the sample's surface. These electrons interact only with the top few atomic layers, producing a diffraction pattern that is observed on a fluorescent screen, as shown in Figure (2.5). This method enables real-time monitoring of surface structures and growth processes.

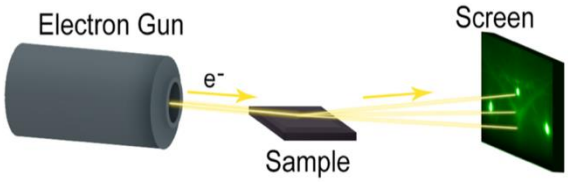

Fig. (2.5): The simplest RHEED.

2.2.4 X-ray diffraction (XRD)

It is a powerful, non-destructive analytical technique used to study the structure of crystalline materials. It is based on Bragg's Law ($n\lambda = 2d\sin\theta$), which describes how X-rays reflect from crystal planes at specific angles. In this method, a monochromatic X-ray beam is directed onto the sample, and the reflected rays are collected by a detector, as shown in Figure (2.6). As the X-rays interact with the orderly atomic planes in a crystal, they produce constructive interference when specific conditions are met, forming a diffraction pattern. This pattern provides valuable information about the crystal structure, crystallinity and defects in the material.[10]

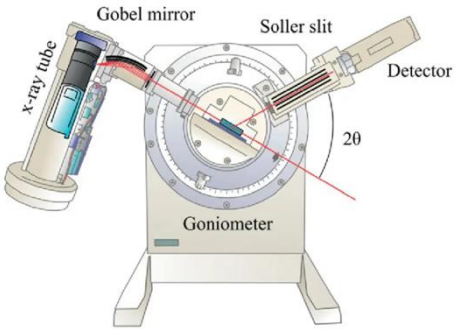

Fig. (2.6): Schematic representation of XRD technique.

2.3 Photoluminescence Spectroscopy (PL)

Photoluminescence spectroscopy (PL) is a non-contact, nondestructive optical technique used to probe the electronic and optical properties of materials. In this technique, light energy (photons) is

directed onto a sample, where it is absorbed, causing the excitation of electrons to higher energy states a process known as photoexcitation. As the excited electrons return to lower energy levels, they release energy in the form of emitted photons. This light emission is called photoluminescence (PL), as shown in Figure (2.7), and analyzing the characteristics of the emitted light can reveal valuable information about a material's band structure, defect states, and overall quality.

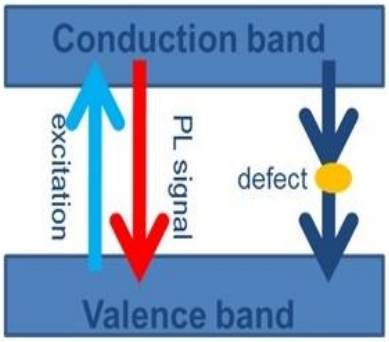

Fig. (2.7): PL signal generation.

Based on the above principle, the PL properties of the as-grown GaN nanorods (NRs) on Si substrates were investigated experimentally as follows: The PL spectra were measured using a continuous-wave (CW) He–Cd laser (KIMMON IK Series) with a wavelength of 325 nm and a fixed power of 18 mW was used as the excitation source as shown in Figure (2.8). The emitted PL signal was collected and dispersed using a one-meter grating monochromator (JASCO CT-100), blazed at 300 nm. To eliminate the influence of scattered laser light from the sample surface, a low-energy pass filter was integrated into the monochromator system. The PL signal was then detected using a photomultiplier tube (PMT, type 650 U) in combination with a lock-in amplifier, significantly improving the signal-to-noise ratio.

Low-temperature measurements were carried out using a closed-cycle helium cryostat (ACTI Cryogenics), which allowed the samples to be cooled down to 10 K. This enabled the observation of temperature-dependent optical behaviors and reduced the thermal broadening of PL peaks. The resulting spectra were analyzed, and a multi-peak analysis was conducted to resolve various emission components, including free exciton recombination, donor–acceptor pair transitions, and emissions related to crystal defects.

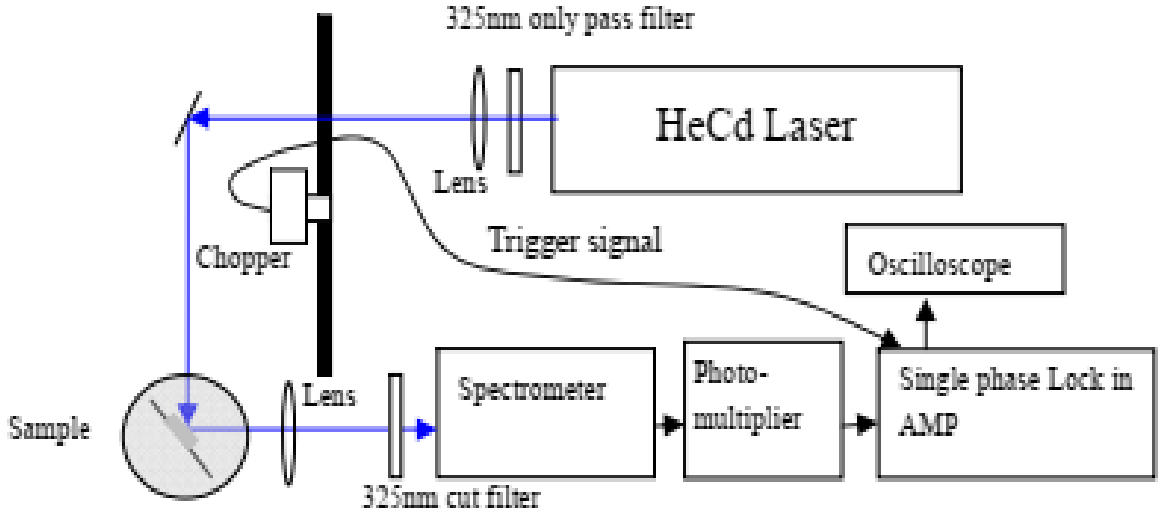

Fig. (2.8): Schematic diagram of the photoluminescence (PL) measurement setup.

Chapter 3

Results and discussion of the heterostructure nanocolumn

3.1 Morphological and structural results

3.1.1 Morphological results

The morphology of the grown heterostructure nanorods with GaN Single Quantum (SQ) disk is confirmed by high-resolution scanning electron microscope (HR-SEM) as shown in Figure (3.1a). The HR- SEM image shows the vertically c-oriented nanorods grown perpendicular to the Si substrate surface. HR-TEM image observations presented in Figure (3.1b) show SQ Disk of GaN nanorod with an average thickness of 3 nm. The estimated average diameter of the grown $Al_{0.12}Ga_{0.88}N$/ GaN/$Al_{0.12}Ga_{0.88}N$/ GaN heterostructure nanocolumn is around 20 nm and the whole nanocolumn length is around 220 nm. These morphological observations using the HR- SEM, and HR-TEM show the vertical growth of heterostructure nanocolumns with a single quantum disk of GaN inserted in $Al_{0.12}Ga_{0.88}N$ nanocolumns.

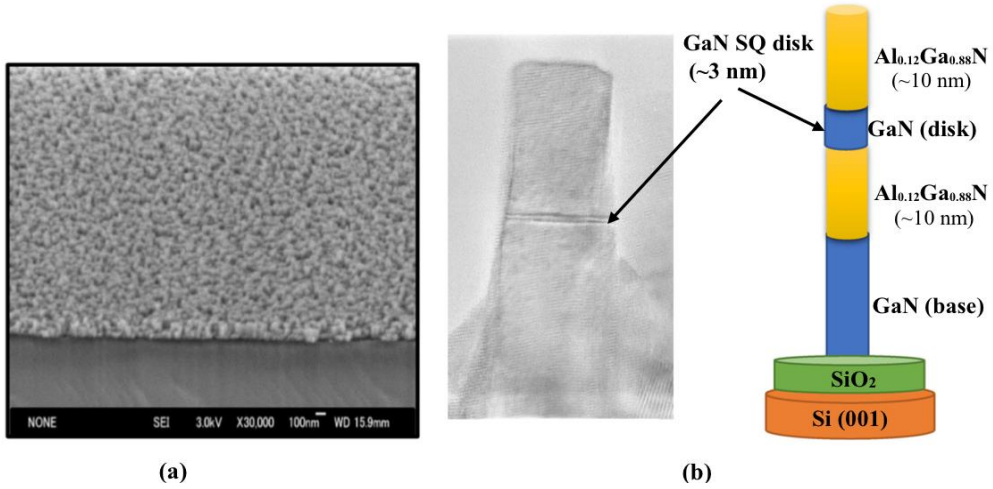

Fig. (3.1): a) FE-SEM and b) HR-TEM images of the Al0.12GaN0.88/GaN/Al0.12GaN0.88/GaN SQ disk nanocolumns.

3.1.2 Structural results

The RHEED patterns of the different stages of the grown $Al_{0.12}GaN_{0.88}$/GaN/$Al_{0.12}GaN_{0.88}$/GaN nanocolumns are shown in Figure (3.2). The presented RHEED patterns help to confirm simultaneously the good structural quality during growth starting with: (a) GaN, (b) $Al_{0.12}Ga_{0.88}N$, (c) GaN single quantum disk and (d) $Al_{0.12}Ga_{0.88}N$ at the top, the broken-ring RHEED patterns indicate that the hexagonal GaN structure is established in the grown nanocolumns with their c-axes perpendicular to the substrate surfaces.

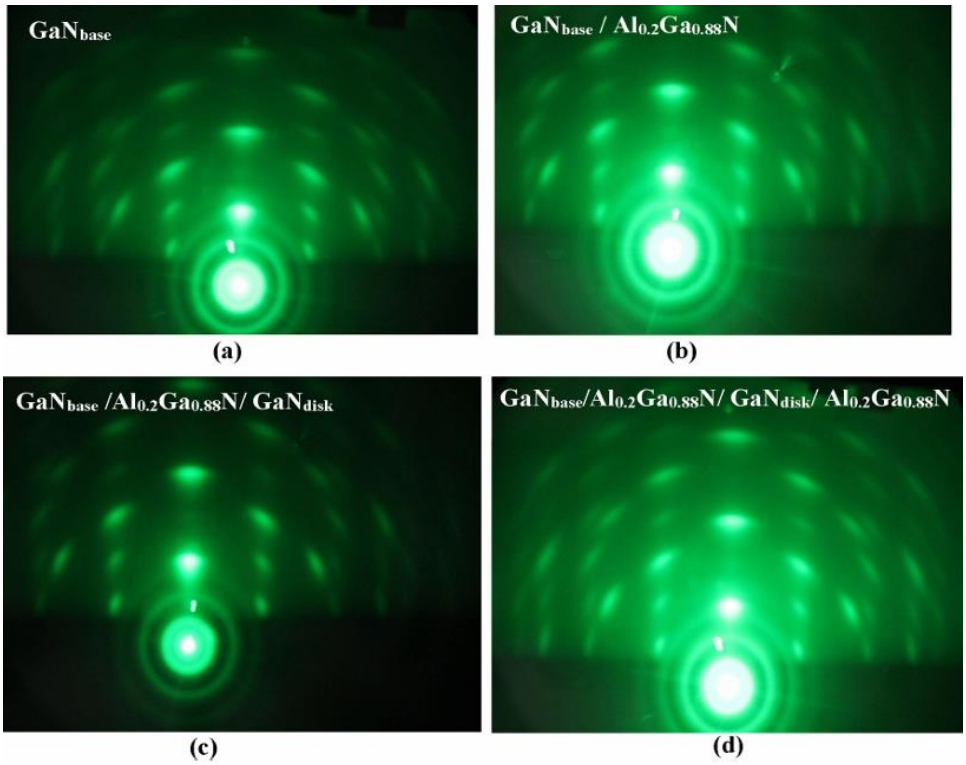

Fig. (3.2): The RHEED patterns of the different stages of the grown single quantum disk nanocolumnar structure: a) GaN base, b) Al0.12GaN0.88 barrier, c) GaN SQ disk and d) Al0.12GaN0.88 top layer.

The XRD pattern of the synthesized sample indicates only three diffraction peaks as shown in Fig (3.3). The first peak corresponds to the Si (111) substrate, confirming the successful growth of nanocolumns on Si. The second peak is indexed to the (002) plane of hexagonal GaN, while the third peak is associated with the (002) plane of hexagonal AlN. No additional peaks are detected in the XRD patterns of AlGaN/GaN/AlGaN nanocolumn indicating that the nanocolumn were produced with high crystalline structure along the c-axis orientation.

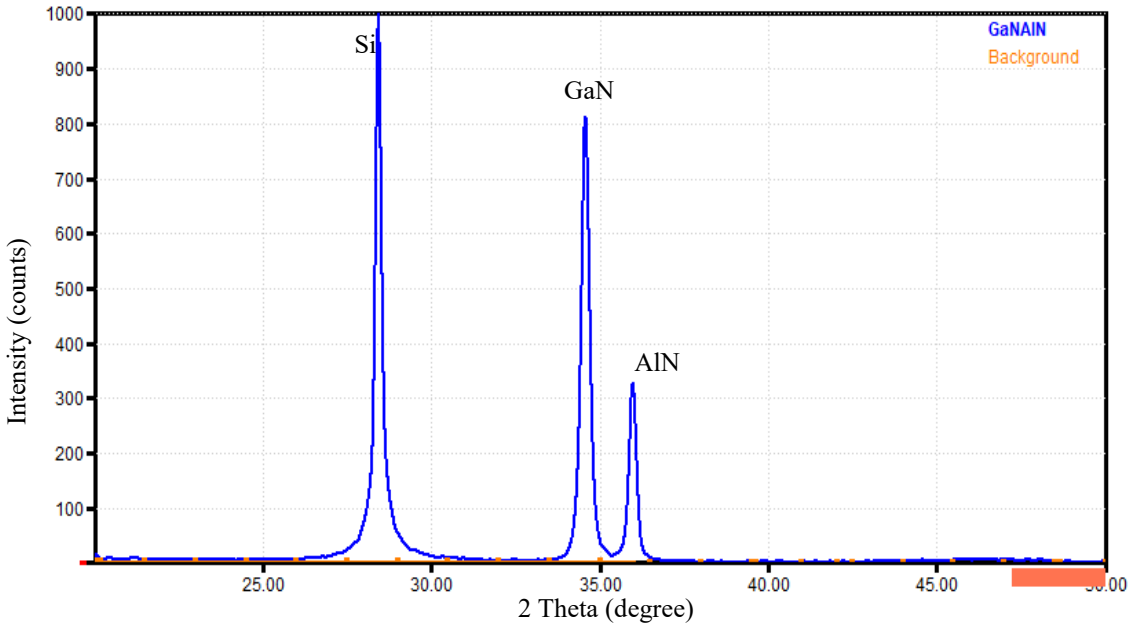

Fig. (3.3): X-ray diffraction patterns of AlGaN/GaN/AlGaN nanocolumn sample.

Therefore, the morphological and structural studies confirmed that the AlGaN/GaN/AlGaN heterostructure nanocolumns were grown on the Si substrate, with single quantum disk of GaN and arranged well vertically in an ordered pattern with high crystalline structure.

3.2 PL results at low temperature

The PL spectra of GaN, AlN/GaN nanorods, and AlGaN/GaN/AlGaN nanocolumns were measured at a low temperature, 10K. A laser beam with a wavelength of 325 nm, corresponding to an energy of about 3.81 eV, was used as a source for excitation. PL spectra for each sample will be presented and discussed below.

3.2.1 PL spectra of GaN nanorods

The PL spectra of GaN nanoroad was measured at 10K and shown in Figure (3.4). The PL spectra show one strong peak at 3.42 eV attributed to donor bound exciton emission close to the surface region. The donor bound exciton emission results from the recombination of an electron hole pair (exciton) bound to a neutral donor impurity within the GaN crystal lattice.

These impurities create localized energy levels slightly below the conduction band of GaN, causing the bound exciton to emit photons with slightly lower energy than those from a free exciton, which typically occurs around 3.48 eV at low temperatures [11].

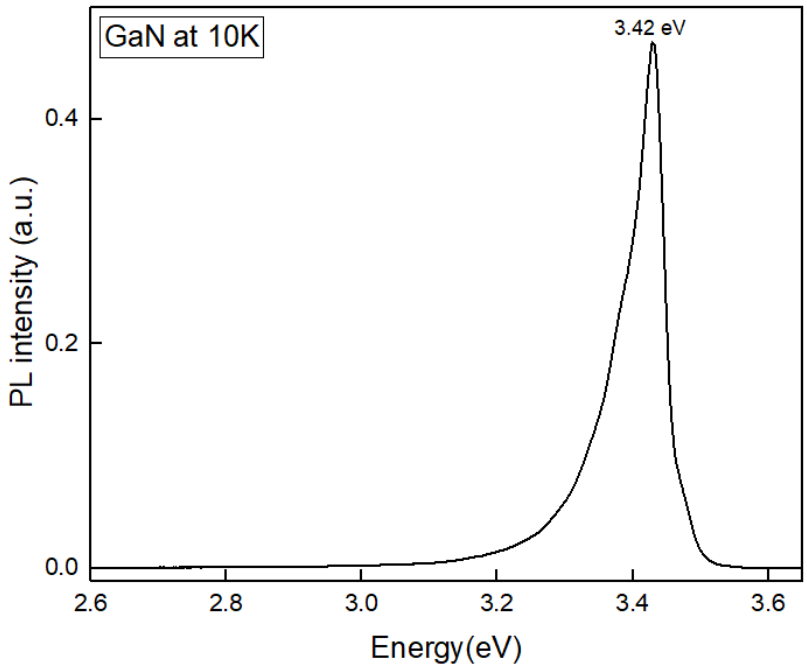

Fig. (3.4): PL spectra of GaN nanorods at 10K.

3.2.2 PL spectra of AlN/GaN nanorods

The PL spectra of AN/GaN nanorod was shown in Figure (3.5). The PL spectra show two dominant peaks: one at 3.38 eV for GaN and is attributed to the bound exciton emissions, and the other at 3.18 eV related to the growth of AlN on the top of GaN which shows broad band emissions.

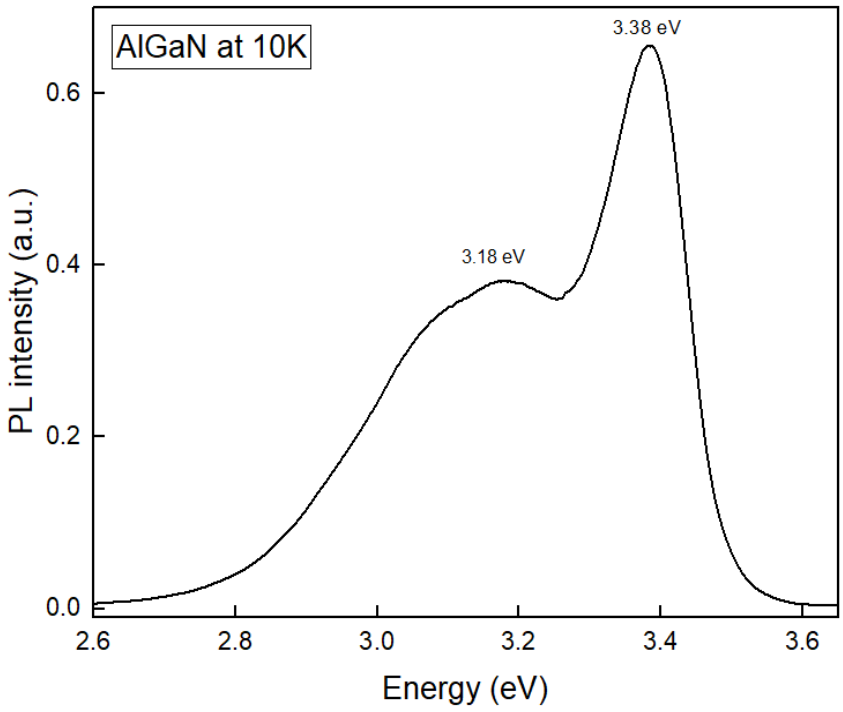

Fig. (3.5): PL spectra of AlN/GaN nanorods at 10K.

These broad emissions at low temperature are attributed to strain resulting from the lattice mismatch between GaN and AlN when AlN is grown on top of GaN. This strain arises from differences in the lattice constants of the two materials: GaN has hexagonal crystal structure with lattice constants of approximately a = 3.19 Å and c = 5.19 Å, while AlN has slightly smaller lattice constants of about; a = 3.11 Å and c = 4.98 Å. As a result, when AlN is deposited on the top of GaN, AlN experiences compressive strain due to the larger lattice dimensions of the underlying GaN layer [12].

3.2.3 PL spectra of AlGaN/GaN/AlGaN nanocolumns

The PL spectra of $Al_{0.12}GaN_{0.88}$/GaN/$Al_{0.12}GaN_{0.88}$/GaN nanocolumns were measured at 10K and shown in Fig. (3.6). The PL spectra show two strong emission peaks at 3.47 eV for GaN attributed to donor bound exciton emission and another peak at 3.53 eV. The higher energy peak is blue shifted by 6 meV relative to the donor bound exciton peak of GaN and is attributed to exciton quantum confinement in GaN quantum disk.

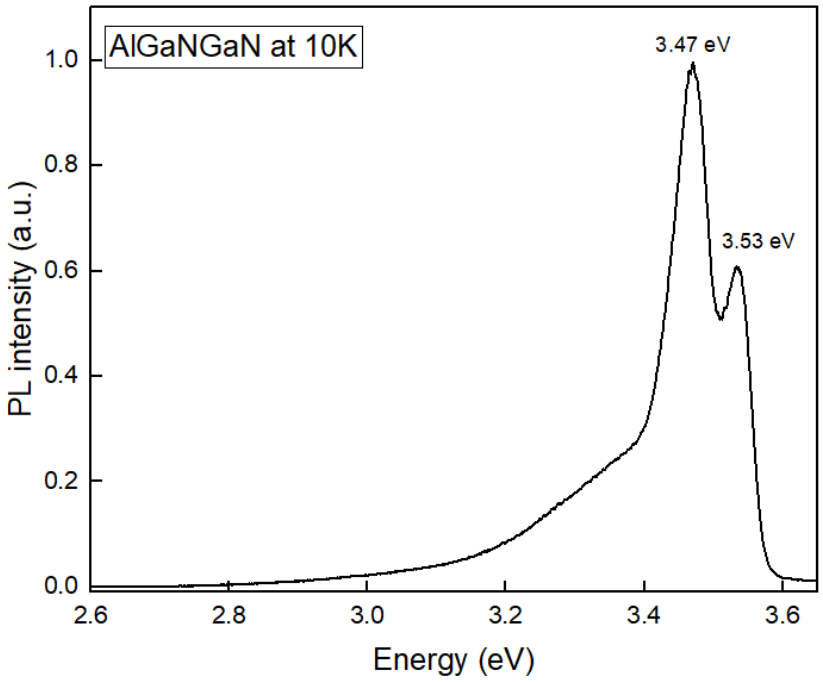

Fig. (3.6): PL spectra of AlGaN/GaN/AlGaN nanocolumn at 10K.

This narrow emission peak confirms the high crystalline quality of the structure and that the quantum disk's energy states are well-defined and free from significant strain. In comparison between GaN nanoroad and AlGaN/GaN/AlGaN nanocolumns is shown in Figure (3.7), confirmed that the emission peak at 3.53eV is attributed to the single quantum disk of GaN. This blue shift confirms the presence of quantum confinement of the excitons within the GaN thin nanolayer (~3nm) led to a higher energy emission compared to bulk GaN (inset figure 3.7). The narrow emission peak indicates the high crystalline quality of the structure, and that the energy states of the quantum disk are well-defined and free from significant strain.

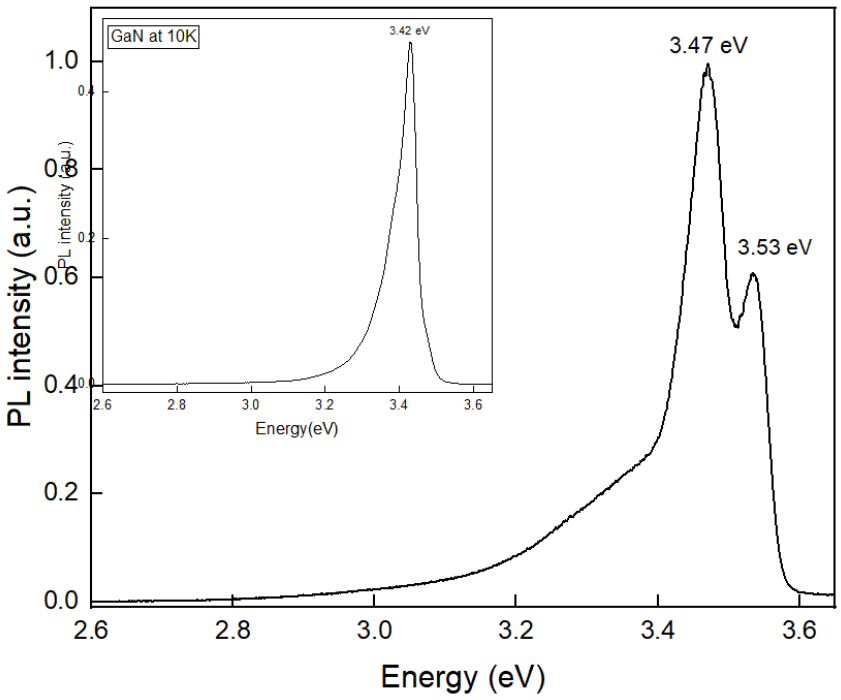

Fig. (3.7): GaN and AlGaN/GaN comparison.

Another important observation of the heterostructure nanocolumns is shown in comparison with AlN/GaN (inset figure 3.8) with the heterostructure nanocolumns and shown in Fig. (3.8). It is clear that, the strain due to AlN growth on the top of GaN is significantly reduced and this is due to the small lattice mismatch between the $Al_{0.12}Ga_{0.88}N$ alloy and GaN layer. Both lattices share the same hexagonal structure, and their lattice constants are very close. Specifically, lattice constant of $Al_{0.12}Ga_{0.88}N$ is around a= 3.12 Å and c = 5.11 Å, resulting in a minimal lattice mismatch between GaN and AlGaN alloy. As a result of the quantum confinement with the higher energy emission at 3.52eV and without stress effect due to the layers growth of the heterostructures nanocolumn.

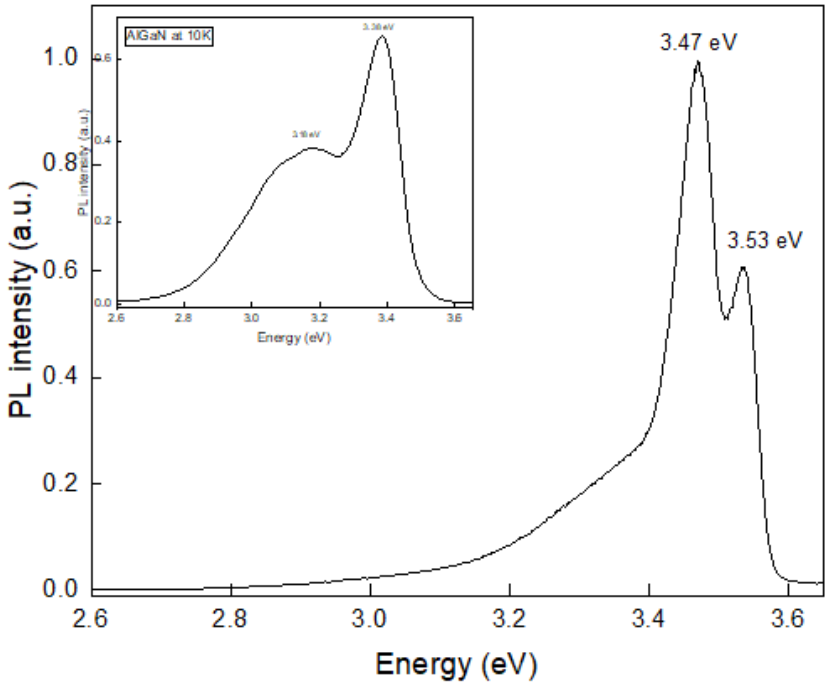

Fig. (3.8): AlGaN and AlGaN/GaN comparison.

CONCLOUSION

AlGaN/GaN/AlGaN heterostructure nanocolumns were grown on a Si substrate with Al concentration of 12% and GaN 88% using Plasma-assisted molecular epitaxy (PA-MBE) technique. The Morphological and structural investigation were done using SEM, TEM, RHEED, and XRD techniques and confirmed the good vertical crystalline growth of the AlGaN/GaN/AlGaN heterostructure nanocolumns on the Si substrate. The Single quantum (SQ) disk with a thickness of around 3 nm was detected by TEM. The PL spectra of the nanocolumns at 10K shows two dominant peaks at 3.47 eV for bulk GaN attributed to bound-donor exciton emission and 3.53 eV for SQ disk GaN at 10K. A low strain effect is observed due to the similar lattice matching between GaN and AlGaN comparing to the high mismatch in AlN/GaN nanorods. Therefore, these results shows the quantum confinement according to the higher energy emission at 3.53 eV and reduce the stress effect due to the layers growth with similar unit cells of the heterostructures nanocolumn where is important in many optoelectronic applications.

REFERENCES

[1] B. Mekuye and B. Abera, "Nanomaterials: An overview of synthesis, classification, characterization, and applications," *Nano Select*, vol. 4, no. 8, pp. 486–501, Aug. 2023, doi: 10.1002/nano.202300038.

[2] Richard J. D. Tilley, *Crystals and Crystal Structures*.

[3] Fabrizio Roccaforte and Mike Leszczynski, *Nitride Semiconductor Technology: Power Electronics and Optoelectronic Devices*.

[4] Elcin Akar, Bruno Cesar da Silva, Matteo Kenel, Martien den Hertog, and Eva Monroy, "Fabrication of Tapered and Cylindrical GaN Nanowires Using Nanosphere Lithography".

[5] E. Akar, I. Dimkou, A. Ajay, Martien I den Hertog, and E. Monroy, "Ultraviolet Photodetectors based on GaN and AlGaN/AIN Nanowire Ensembles: Effects of Planarization with Hydrogen Silsesquioxane and Nanowire Architecture".

[6] M. A. Reshchikov, "Photoluminescence from Vacancy-Containing Defects in GaN," May 01, 2023, *John Wiley and Sons Inc*. doi: 10.1002/pssa.202200402.

[7] L. H. Robins, K. A. Bertness, J. M. Barker, N. A. Sanford, and J. B. Schlager, "Optical and structural study of GaN nanowires grown by catalyst-free molecular beam epitaxy. I. Near-band-edge luminescence and strain effects," *J Appl Phys*, vol. 101, no. 11, 2007, doi: 10.1063/1.2736264.

[8] A. Wojcik *et al.*, "Photoreflectance study of GaN/AlGaN structures," in *Physica Status Solidi C: Conferences*, Wiley-VCH Verlag, Dec. 2002, pp. 491–494. doi: 10.1002/pssc.200390096.

[9] N. AbdelAll, J. ElGhoul, and M. Almokhtar, "Low temperature photoluminescence study of AlxGa1−xN/GaN/AlxGa1−xN heterostructure nanocolumns," *Journal of Materials Science: Materials in Electronics*, vol. 34, no. 21, Jul. 2023, doi: 10.1007/s10854-023-11003-7.

[10] J. P. Patel and P. H. Parsania, "Characterization, testing, and reinforcing materials of biodegradable composites," *Biodegradable and Biocompatible Polymer Composites: Processing, Properties and Applications*, pp. 55–79, Jan. 2017, doi: 10.1016/B978-0-08-100970-3.00003-1.

[11] M. Almokhtar, N. A. All, J. Q. M. Almarashi, and H. Asahi, “Photoluminescence enhancement associated with the small size of GaN nanorods,” *J Alloys Compd*, vol. 894, Feb. 2022, doi: 10.1016/j.jallcom.2021.162408.

[12] N. Abdel All, “Structural and photoluminescence study of thin GaN and AlN/GaN nanowires,” *Journal of Materials Science: Materials in Electronics*, vol. 34, no. 10, Apr. 2023, doi: 10.1007/s10854-023-10297-x.